# Paper review
# &
# Study about radiative charm decay

Department of Physics, Yonsei Univ.

**Jaeyoung Kim** (jaeyoung97@yonsei.ac.kr)

2022.01.14.

# Introduction

Title: Observation of $\boldsymbol{D^0 \to \rho^0\gamma}$ and **Search for CP violation** in **Radiative Charm Decays** (Phys. Rev. Lett. 118, 051801 (2017))

Abstract:

1. First observation of $D^0 \to \rho^0\gamma$

2. First search for CP violation in decays $D^0 \to \rho^0\gamma, \phi\gamma, \overline{K}^{*0}(892)\gamma$ using $943fb^{-1}$ Belle data

3. Improved measurement of $B(D^0 \to \phi\gamma), B(D^0 \to \overline{K}^{*0}\gamma)$

# Introduction

| $D^0$ | Radiative modes | | |
|---|---|---|---|
| $\rho^0\gamma$ | $(\ 1.82\ \pm\ 0.32\ ) \times 10^{-5}$ | | |
| $\omega\gamma$ | $<\ 2.4\ \times 10^{-4}$ | CL=90% | |
| $\phi\gamma$ | $(\ 2.81\ \pm\ 0.19\ ) \times 10^{-5}$ | | |
| $\overline{K}^*(892)^0\gamma$ | $(\ 4.1\ \pm\ 0.7\ ) \times 10^{-4}$ | | |

Charm physics:

- At the $\Upsilon(4S)$ resonance,

| Charm production | cross section |
|---|---|
| $c\bar{c}$ | 1.3nb |
| $\Upsilon(4S) \to B \to D$ | 1.1nb |

➡ expected # of D mesons production $\approx 10^9$ per $ab^{-1}$ of data

- The decay chains used in this analysis are $D^{*+} \to D^0\pi^+$,
  $D^0 \to \phi\gamma \to K^+K^-\gamma$ ,
  $D^0 \to \overline{K}^{*0}\gamma \to K^-\pi^+\gamma$ ,
  $D^0 \to \rho^0\gamma \to \pi^+\pi^-\gamma$ ,
  $(D^0 \to \omega\gamma \to \pi^+\pi^-\gamma)$
- Vector mesons' decay:

$B(\phi \to K^+K^-) = 49\%$, $B\left(\phi \to K_L^0K_S^0\right) = 34\%$??

$B(\overline{K}^{*0} \to K^+\pi^-) \sim 100\%$

$B(\rho^0 \to \pi^+\pi^-) \sim 100\%$

# Introduction

- Charge-conjugate modes are also included in the chain $D^{*+} \to D^0\pi^+$,
  $D^0 \to \phi\gamma \to K^+K^-\gamma$ ,
  $D^0 \to \bar{K}^{*0}\gamma \to K^-\pi^+\gamma$ ,
  $D^0 \to \rho^0\gamma \to \pi^+\pi^-\gamma$

- $B(D^{*+} \to D^0\pi^+) = 67.7\%$

- $\sigma(e^+e^- \to c\bar{c} \to D^{*+}X) = 597pb$(X is anything)

➡ expected # of $D^{*+}$ mesons $\approx 10^8$ per $ab^{-1}$ of data

➡ sufficiently high to ensure a statistics of $D^0$ sample

# Introduction

Ref: Belle II physics book (Table 123.)

**Table 123.** The "golden channels" for charm physics.

| Channel | Observable | Belle/BaBar measurement | | Scaled | |
|---|---|---|---|---|---|
| | | $\mathcal{L}$ [ab$^{-1}$] | Value | 5 ab$^{-1}$ | 50 ab$^{-1}$ |
| Leptonic decays | | | | | |
| $D_s^+ \to \ell^+\nu$ | $\mu^+$ events | 0.913 | $492 \pm 26$ | 2.7k | 27k |
| | $\tau^+$ events | | $2217 \pm 83$ | 12.1k | 121k |
| | $f_{D_s}$ | | 2.5% | 1.1% | 0.34% |
| $D^+ \to \ell^+\nu$ | $\mu^+$ events | — | — | 125 | 1250 |
| | $f_D$ | — | — | 6.4% | 2.0% |
| Rare and radiative decays | | | | | |
| $D^0 \to \rho^0\gamma$ | $A_{CP}$ | 0.943 | $+0.056 \pm 0.152 \pm 0.006$ | $\pm 0.07$ | $\pm 0.02$ |
| $D^0 \to \phi\gamma$ | $A_{CP}$ | | $-0.094 \pm 0.066 \pm 0.001$ | $\pm 0.03$ | $\pm 0.01$ |
| $D^0 \to \overline{K}^{*0}\gamma$ | $A_{CP}$ | | $-0.003 \pm 0.020 \pm 0.000$ | $\pm 0.01$ | $\pm 0.003$ |
| Mixing and indirect (time-dependent) CP violation | | | | | |
| $D^0 \to K^+\pi^-$ (no CPV) | $x'^2$ (%) | 0.976 | $0.009 \pm 0.022$ | $\pm 0.0075$ | $\pm 0.0023$ |
| | $y'$ (%) | | $0.46 \pm 0.34$ | $\pm 0.11$ | $\pm 0.035$ |
| (CPV allowed) | $\lvert q/p\rvert$ | World avg. [230] | $0.89^{+0.08}_{-0.07}$ | $\pm 0.20$ | $\pm 0.05$ |
| | $\phi$ (°) | with LHCb | $-12.9^{+9.9}_{-8.7}$ | $\pm 16°$ | $\pm 5.7°$ |
| $D^0 \to K^+\pi^-\pi^0$ | $x''$ | 0.384 | $2.61^{+0.57}_{-0.68} \pm 0.39$ | — | $\pm 0.080$ |
| | $y''$ | | $-0.06^{+0.55}_{-0.64} \pm 0.34$ | — | $\pm 0.070$ |
| $D^0 \to K^0_S\pi^+\pi^-$ | $x$ (%) | 0.921 | $0.56 \pm 0.19^{+0.04\,+0.06}_{-0.08\,-0.08}$ | $\pm 0.16$ | $\pm 0.11$ |
| | $y$ (%) | | $0.30 \pm 0.15^{+0.04\,+0.03}_{-0.05\,-0.07}$ | $\pm 0.10$ | $\pm 0.05$ |
| | $\lvert q/p\rvert$ | | $0.90^{+0.16\,+0.05\,+0.06}_{-0.15\,-0.04\,-0.05}$ | $\pm 0.12$ | $\pm 0.07$ |
| | $\phi$ (°) | | $-6 \pm 11 \pm 3^{+3}_{-4}$ | $\pm 8$ | $\pm 4$ |
| Direct (time-integrated) CP violation in % | | | | | |
| $D^0 \to K^+K^-$ | $A_{CP}$ | 0.976 | $-0.32 \pm 0.21 \pm 0.09$ | $\pm 0.10$ | $\pm 0.03$ |
| $D^0 \to \pi^+\pi^-$ | $A_{CP}$ | 0.976 | $+0.55 \pm 0.36 \pm 0.09$ | $\pm 0.16$ | $\pm 0.05$ |
| $D^0 \to \pi^0\pi^0$ | $A_{CP}$ | 0.966 | $-0.03 \pm 0.64 \pm 0.10$ | $\pm 0.28$ | $\pm 0.09$ |
| $D^0 \to K^0_S\pi^0$ | $A_{CP}$ | 0.966 | $-0.21 \pm 0.16 \pm 0.07$ | $\pm 0.08$ | $\pm 0.02$ |
| $D^0 \to K^0_S K^0_S$ | $A_{CP}$ | 0.921 | $-0.02 \pm 1.53 \pm 0.17$ | $\pm 0.66$ | $\pm 0.23$ |
| $D^0 \to K^0_S\eta$ | $A_{CP}$ | 0.791 | $+0.54 \pm 0.51 \pm 0.16$ | $\pm 0.21$ | $\pm 0.07$ |
| $D^0 \to K^0_S\eta'$ | $A_{CP}$ | 0.791 | $+0.98 \pm 0.67 \pm 0.14$ | $\pm 0.27$ | $\pm 0.09$ |
| $D^0 \to \pi^+\pi^-\pi^0$ | $A_{CP}$ | 0.532 | $+0.43 \pm 1.30$ | $\pm 0.42$ | $\pm 0.13$ |
| $D^0 \to K^+\pi^-\pi^0$ | $A_{CP}$ | 0.281 | $-0.60 \pm 5.30$ | $\pm 1.26$ | $\pm 0.40$ |
| $D^0 \to K^+\pi^-\pi^+\pi^-$ | $A_{CP}$ | 0.281 | $-1.80 \pm 4.40$ | $\pm 1.04$ | $\pm 0.33$ |
| $D^+ \to \phi\pi^+$ | $A_{CP}$ | 0.955 | $+0.51 \pm 0.28 \pm 0.05$ | $\pm 0.12$ | $\pm 0.04$ |
| $D^+ \to \pi^+\pi^0$ | $A_{CP}$ | 0.921 | $+2.31 \pm 1.24 \pm 0.23$ | $\pm 0.54$ | $\pm 0.17$ |
| $D^+ \to \eta\pi^+$ | $A_{CP}$ | 0.791 | $+1.74 \pm 1.13 \pm 0.19$ | $\pm 0.46$ | $\pm 0.14$ |
| $D^+ \to \eta'\pi^+$ | $A_{CP}$ | 0.791 | $-0.12 \pm 1.12 \pm 0.17$ | $\pm 0.45$ | $\pm 0.14$ |
| $D^+ \to K^0_S\pi^+$ | $A_{CP}$ | 0.977 | $-0.36 \pm 0.09 \pm 0.07$ | $\pm 0.05$ | $\pm 0.02$ |
| $D^+ \to K^0_S K^+$ | $A_{CP}$ | 0.977 | $-0.25 \pm 0.28 \pm 0.14$ | $\pm 0.14$ | $\pm 0.04$ |
| $D_s^+ \to K^0_S\pi^+$ | $A_{CP}$ | 0.673 | $+5.45 \pm 2.50 \pm 0.33$ | $\pm 0.93$ | $\pm 0.29$ |
| $D_s^+ \to K^0_S K^+$ | $A_{CP}$ | 0.673 | $+0.12 \pm 0.36 \pm 0.22$ | $\pm 0.15$ | $\pm 0.05$ |

# Introduction

Ref: Belle II physics book
(Table 123.)

**Table 123.** The "golden channels" for charm physics.

| Channel | Observable | Belle/BaBar measurement | | Scaled | |
|---|---|---|---|---|---|
| | | $\mathcal{L}$ [ab$^{-1}$] | Value | 5 ab$^{-1}$ | 50 ab$^{-1}$ |
| Rare and radiative decays | | | | | |
| $D^0 \to \rho^0 \gamma$ | $A_{CP}$ | 0.943 | $+0.056 \pm 0.152 \pm 0.006$ | $\pm 0.07$ | $\pm 0.02$ |
| $D^0 \to \phi \gamma$ | $A_{CP}$ | | $-0.094 \pm 0.066 \pm 0.001$ | $\pm 0.03$ | $\pm 0.01$ |
| $D^0 \to \overline{K}^{*0} \gamma$ | $A_{CP}$ | | $-0.003 \pm 0.020 \pm 0.000$ | $\pm 0.01$ | $\pm 0.003$ |

Result of this paper

# Introduction

- Branching fractions of radiative decay modes:

| $D^0$ | Radiative modes | | |
|---|---|---|---|
| $\rho^0\gamma$ | $(\ 1.82\ \pm\ 0.32\ ) \times 10^{-5}$ | | |
| $\omega\gamma$ | $<\ 2.4\ \times 10^{-4}$ | CL=90% | |
| $\phi\gamma$ | $(\ 2.81\ \pm\ 0.19\ ) \times 10^{-5}$ | | |
| $\overline{K}^*(892)^0\gamma$ | $(\ 4.1\ \pm\ 0.7\ ) \times 10^{-4}$ | | |

Ref: 2021 PDG

In this paper,
$B(D^0 \to \rho^0\gamma) = (1.77 \pm 0.30 \pm 0.07) \times 10^{-5}$,
➡ Observation
$B(D^0 \to \phi\gamma) = (2.76 \pm 0.19 \pm 0.10) \times 10^{-5}$,
$B(D^0 \to \overline{K}^{*0}\gamma) = (4.66 \pm 0.21 \pm 0.21) \times 10^{-4}$
➡ Improved measurements

- Properties:

| | meson | constituents | | Mass(MeV) |
|---|---|---|---|---|
| Charmed (C=1, S=B′=0) | $D^0$ | $c\bar{u}$ | $I(J^P) = 1/2(0^-)$ | 1864 |
| Unflavored (S=C=B′=0) | $\rho^0$ | $\frac{u\bar{u} - d\bar{d}}{\sqrt{2}}$ | $I^G(J^{PC}) = 1^+(1^{--})$ | 775 |
| | $\omega$ | $\frac{u\bar{u} + d\bar{d}}{\sqrt{2}}$ | $I^G(J^{PC}) = 0^-(1^{--})$ | 782 |
| | $\phi$ | $s\bar{s}$ | $I^G(J^{PC}) = 0^-(1^{--})$ | 1019 |
| Strange (S=1, C=B′=0) | $\overline{K}^{*0}$ | $s\bar{d}$ | $I(J^P) = 1/2(1^-)$ | 892 |

# Motivations for the analysis

Within the standard model (SM), charge-parity ($CP$) violation in weak decays of hadrons arises due to a single irreducible phase in the ① Cabibbo-Kobayashi-Maskawa matrix [1] and is expected to be very small for charmed hadrons: up to a few $10^{-3}$ [2–4]. Observation of $CP$ violation above the SM expectation would be an indication of new physics. This phenomenon in the charm sector has been extensively probed in the past decade in many different decays [5], reaching a sensitivity below 0.1% in some cases [6]. The search for $CP$ violation in radiative charm decays is complementary to the searches that have been exclusively performed in hadronic or leptonic decays. Theoretical calculations [7,8] show that, in SM extensions ② with chromomagnetic dipole operators, sizable $CP$ asymmetries can be expected in $D^0 \to \phi\gamma$ and $\rho^0\gamma$ decays. No ③ experimental results exist to date regarding $CP$ violation in any of the radiative $D$ decays.

Motivation for physics:

① Very small CKM elements for charmed Hadrons

② charm decays: FCNC(Flavor-Changing with neutral current) (ΔC=1)

- Hadronic contributions to weak decays are hard to calculate(Non-perturbative QCD)
- Long-distance effects are dominant, and theoretically difficult

③ GIM cancellation

# Motivations for the analysis

④ Radiative charm decays are dominated by long-range nonperturbative processes that can enhance the branching fractions up to $10^{-4}$, whereas short-range interactions are predicted to yield rates at the level of $10^{-8}$ [9,10]. ⑤ Measurements of branching fractions of these decays can therefore be used to test the QCD-based calculations of long-distance dynamics. The radiative decay $D^0 \to \phi\gamma$ was first observed by Belle [11] and later measured with increased precision by *BABAR* [12]. In the same study, *BABAR* made the observation of $D^0 \to \bar{K}^{*0}(892)\gamma$. As for $D^0 \to \rho^0\gamma$, CLEO II has set an upper limit on its branching fraction at $2 \times 10^{-4}$ [13].

⑥ Next slide

④⑤ → ②

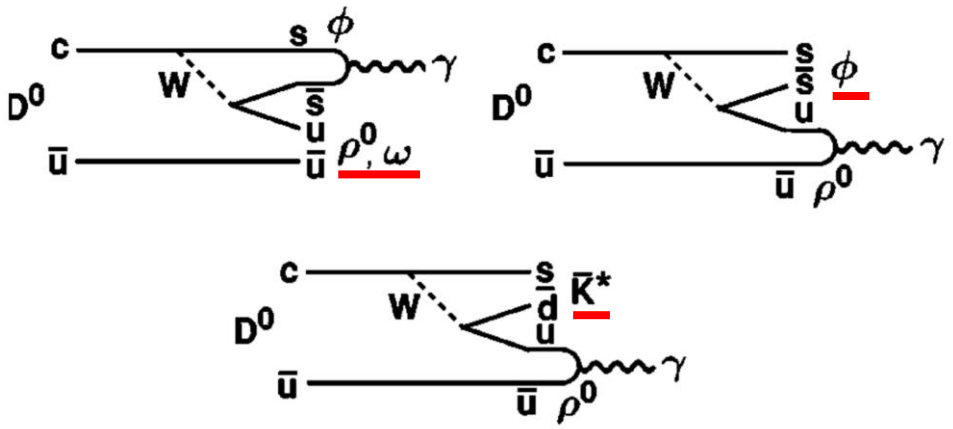


FIG. 1. Feynman diagrams for the long distance electromagnetic contributions.

Ref: CLEO II paper (1998)

# Motivations for the analysis

## ⑥ Experimental History of radiative charm decay

- CLEO II(1998) conducted a search for $D^0 \to V\gamma$, for $V = \phi, \bar{K}^{*0}, \rho^0, \omega$

Due to limited statistics(4.8 $fb^{-1}$ data sample), they were unable to observe any of modes

TABLE I. The upper limit yields extracted from the likelihood fit and the resulting 90% confidence level upper limits on the branching fractions incorporating systematic uncertainties in yield and efficiency determination.

| Mode | $D^0 \to \phi\gamma$ | $D^0 \to \omega\gamma$ | $D^0 \to \bar{K}^*\gamma$ | $D^0 \to \rho\gamma$ |
|---|---|---|---|---|
| 90% C.L. upper limit yield | 8.9 | 7.7 | 38.5 | 21.6 |
| Detection efficiency (%) | 5.57±0.13% | 2.10±0.05% | 5.51±0.13% | 5.83±0.13% |
| Branching fraction 90% C.L. upper limit | $1.9\times10^{-4}$ | $2.4\times10^{-4}$ | $7.6\times10^{-4}$ | $2.4\times10^{-4}$ |
| Theoretical prediction [4–8] | $0.01-0.34\times10^{-4}$ | $0.01-0.09\times10^{-4}$ | $0.7-8.0\times10^{-4}$ | $0.01-0.63\times10^{-4}$ |

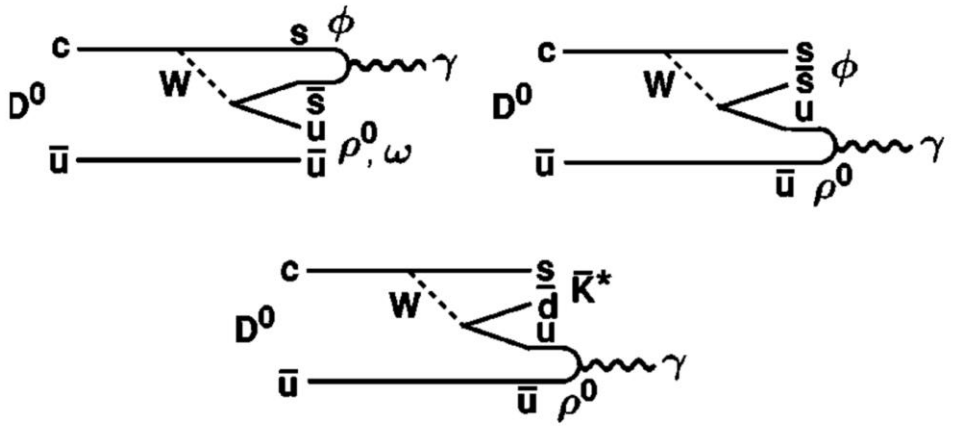


FIG. 1. Feynman diagrams for the long distance electromagnetic contributions.

PRD 58, 092001(1998)

# Motivations for the analysis

⑥ **Experimental History of radiative charm decay**

- Belle(2004): radiative decays of charmed mesons observed for first time

They published a measurement of branching fraction of $D^0 \to \phi\gamma$, based on $78 fb^{-1}$ (Phys. Rev. Lett. 92, 101803)

- BaBar(2008): They reported an observation and branching fraction measurement of $D^0 \to \phi\gamma, D^0 \to \overline{K}^{*0}\gamma$ based on $387.1 fb^{-1}$ (Phys. Rev. D 78, 071101)

- Belle(2017): This paper is next paper to the BaBar(2008)

# Analysis overview

- Measurements are based on $\boldsymbol{943 fb^{-1}}$ Belle data

- Relevant detector components:

**I. Tracking system**(Silicon vertex detector, 50-layter CDC)

**II. PID**( Barrel-like arrangement of TOF scintillation counters, array of aerogel threshold Chrenkov counters, CsI(Tl) crystal-based ECL )

- Use MC events, generated using **EVTGEN, JETSET, and PHTOS** followed by GEANT3

- Figure of merit for optimization: **maximizing** $\frac{S}{\sqrt{S+B}}$ in a signal window of reconstructed invariant $M(D^0)$, $1.8 < M(D^0) < 1.9$ GeV/$c^2$

- Used Branching fraction decay modes **in simulations**: $D^0 \to \rho^0\gamma = 3 \times 10^{-5}$, others use world-average values ??

# Analysis overview

- Reconstruction of $D^0$ mesons by combining a $\boldsymbol{\rho^0, \phi, \bar{K}^{*0}}$ **with a photon**

- Charged particles :

They are reconstructed in **tracking system**.
**Likelihood ratio** for a given track to be **a kaon or pion** is obtained by utilizing specific ionization in the central drift chamber, light yield from aerogel threshold Cherenkov counters, and information from TOF scintillation counters.

- Photons:

Photons require **energy at least 540MeV**
To suppression events with **daughter photons from a $\boldsymbol{\pi^0}$ decay forming a merged cluster**, this analysis **restrict ratio of energy** $\boldsymbol{\frac{E_9}{E_{25}} > 0.94}(E_9: 3 \times 3\ array\ of\ ECL\ crystals)$
→ 63% merged clusters are rejected by this requirement

# Selection and reconstruction of signal decays

- Retain candidate $\boldsymbol{\rho^0}, \boldsymbol{\phi}, \boldsymbol{\bar{K}^{*0}}$ **resonances** if their invariant masses are within 150, 11, $60 MeV/c^2$ of their nominal masses(?)

- $D^0$

$D^0$ should be from $D^{*+}$ to **define $\boldsymbol{D^0}$ flavor** and **suppress combinatorial background**
$D^0$ daughters are **refitted to a common vertex**
**$\boldsymbol{D^0}$ and pion** from $D^{*+}$ are constrained to originate from **a common point within interaction point region**

- Suppression of Combinatorial background

Restrict energy($q = M(\mathrm{D}^{*0}) - M(\mathrm{D}^0) - m(\pi)$ ) released in decay to lie in $0.6 MeV/c^2$ window around nominal mass

- Require $P_{CMS}(D^{*+})$ to exceed 2.72, 2.42, 2.17 GeV/c in $\rho^0\gamma, \phi\gamma, \bar{K}^{*0}\gamma$

# Measurements ($Br, A_{CP}$)

- In this analysis, the paper **didn't perform an absolute measurement**, but **instead a relative calculation using normalization channels** for both $Br, A_{CP}$

- **Normalization modes**:

For $\phi$ mode, $D^0 \to K^+K^-$
For $\bar{K}^{*0}$ mode, $D^0 \to K^-\pi^+$
For $\rho^0$ mode, $D^0 \to \pi^+\pi^-$

- **Branching fraction of signal**

$$B_{sig} = B_{norm} \times \frac{N_{sig}}{N_{norm}} \times \frac{\epsilon_{norm}}{\epsilon_{sig}}$$

$\epsilon =$ reconstruction efficiency

?? We measure the branching fractions and $CP$ asymmetries of the aforementioned radiative decays relative to well-measured hadronic $D^0$ decays to $\pi^+\pi^-$, $K^+K^-$, and $K^-\pi^+$ for the $\rho^0$, $\phi$, and $\bar{K}^{*0}$ mode, respectively. The signal

The analysis of the normalization modes relies on the previous analysis by Belle [31]. The same selection criteria as for signal modes for PID, vertex fit, $q$, and $p_{\mathrm{CMS}}(D^{*+})$ are applied. The signal yield is extracted by subtracting the

[31]: Search for a CP asymmetry in Cabibbo-suppressed $D^0$ decays

# Measurements $(Br, A_{CP})$

??

$$A_{raw} = \frac{N(D^0 - f) - N(\bar{D}^0 - \bar{f})}{N(D^0 - f) + N(\bar{D}^0 - \bar{f})}$$

$$A_{CP} = \frac{B(D^0 - f) - B(\bar{D}^0 - \bar{f})}{B(D^0 - f) + B(\bar{D}^0 - \bar{f})}$$

- $A_{raw} = A_{CP} + A_{FB} + A_{\epsilon}^{\pm}$

$A_{FB}$: forward-backward production symmetry

$A_{\epsilon}^{\pm}$: asymmetry due to reconstruction efficiencies for $\pm$ charged particles

$A_{FB}$, $A_{\epsilon}^{\pm}$ can eliminated by using normalization mode

$\rightarrow A_{raw} = A_{CP} + \cancel{A_{FB}} + \cancel{A_{\epsilon}^{\pm}}$

- $A_{raw}^{sig} - A_{CP}^{sig} = A_{raw}^{norm} - A_{CP}^{norm}$

$\rightarrow A_{CP}^{sig} = A_{raw}^{sig} - A_{raw}^{norm} + A_{CP}^{norm}$

# Background

**Dominant background from $\pi^0$ ($\eta$) veto**

$\pi^0$veto:

- $\pi^0$ subsequently decaying to $\gamma\gamma$ (e.g. $D^0 \to \phi\pi^0, (\pi^0 \to \gamma\gamma)$ )
- If one of daughter photons is missed in reconstruction, final states mimics signal decay

(e.g. $D^0 \to \phi\gamma$)

→ Suppress them by $\pi^0$veto in form of NN(neural network)

- NN is constructed from two mass-veto variables

$\eta$ veto:

- It is similar to $\pi^0$veto
- But it is found to be ineffective due to larger $m_\eta$,

which shifts background further away from signal peak

The signal photon is paired for the first (second) time with all other photons in the event having an energy greater than 30 (75) MeV. The pair in each set whose diphoton invariant mass lies closest to $m(\pi^0)$ is fed to the network. The final criterion on the veto variable rejects about 60% of background while retaining 85% of signal. With this method, we reject 13% more background at the same signal efficiency as compared to the veto used in previous Belle analyses [27]. A similar veto is considered for background from $\eta \to \gamma\gamma$, but is found to be ineffective due to the larger $\eta$ mass, which shifts the background further away from the signal peak.

# Background

**Irreducible background in $\rho^0(\bar{K}^{*0})$ mode**

I. $\pi^+\pi^-(K^-\pi^+)$ with the photon being emitted as final state radiation(FSR)
II. $K^-\rho^+$ with the photon arising from radiative decay of $\rho^+$ ??

$B(\rho^\pm \to \pi^\pm\pi^0) \approx 100\%$
$B(\rho^\pm \to \pi^\pm\gamma) \approx (4.5 \pm 0.5) \times 10^{-4}$

majority of daughter particles. In the $\rho^0$ ($\bar{K}^{*0}$) mode, there are two additional small backgrounds: $\pi^+\pi^-(K^-\pi^+)$ with the photon being emitted as final state radiation (FSR), and $K^-\rho^+$ with the photon arising from the radiative decay of the charged $\rho$ meson. As there are no missing particles, these decays exhibit the same $M(D^0)$ distribution as the signal decays. We jointly denote them as irreducible background. Their yields are fixed to MC expectations

# Signal Extraction and Fit

① We extract the signal yield and $CP$ asymmetry via a simultaneous unbinned extended maximum likelihood fit of $D^0$ and $\bar{D}^0$ samples to the invariant mass of the $D^0$ ② candidates and the cosine of the helicity angle $\theta_H$. The latter is the angle between the momenta of the $D^0$ and the $\pi^+$, $K^+$, or $K^-$ in the rest frame of the $\rho^0$, $\phi$, or $\bar{K}^{*0}$, respectively. By angular momentum conservation, the signal $\cos\theta_H$ distribution depicts a $1-\cos^2\theta_H$ dependence; no background contribution is expected to exhibit a similar shape. For the $\rho^0$ and $\bar{K}^{*0}$ modes, we restrict the helicity angle range to $-0.8 < \cos\theta_H < 0.4$ to suppress backgrounds that peak at the edges of the distribution. For the $\phi$ mode, where the background levels are lower overall, the entire $\cos\theta_H$ range is used. The $D^0$ candidate mass is restricted to $1.67 < M(D^0) < 2.06\ \mathrm{GeV}/c^2$ for all three signal channels.

① • Unbinned likelihood fit
  I. Fit **each single data** point $x_i$
  II. Fit **only functional shape**

• Extended likelihood fit
  I. Add **Poisson fluctuations** for observed events

$$L(x|\theta) = e^{-\mu}\frac{\mu^N}{N!}\prod_{i=1}^{N} f(x_i|\theta)$$

$x$ = measured variable
$\theta$ = unknown parameter
$N$ = recorded events
$\mu$ = average

② • Invariant mass of $D^0$: $M(D^0)$
  • $\cos\theta_H$, where $\theta_H$ is

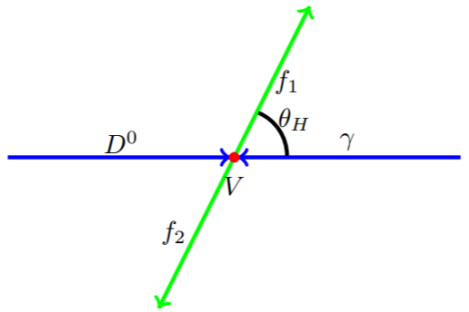


Figure 20: Definition of the helicity angle.

# Signal Extraction and Fit

We extract the signal yield and $CP$ asymmetry via a simultaneous unbinned extended maximum likelihood fit of $D^0$ and $\bar{D}^0$ samples to the invariant mass of the $D^0$ candidates and the cosine of the helicity angle $\theta_H$. The latter is the angle between the momenta of the $D^0$ and the $\pi^+$, $K^+$, or $K^-$ in the rest frame of the $\rho^0$, $\phi$, or $\bar{K}^{*0}$, respectively. By angular momentum conservation, the signal $\cos\theta_H$ distribution depicts a $1-\cos^2\theta_H$ dependence; no background contribution is expected to exhibit a similar shape. For the $\rho^0$ and $\bar{K}^{*0}$ modes, we restrict the helicity angle range to $-0.8 < \cos\theta_H < 0.4$ to suppress backgrounds that peak at the edges of the distribution. For the $\phi$ mode, where the background levels are lower overall, the entire $\cos\theta_H$ range is used. The $D^0$ candidate mass is restricted to $1.67 < M(D^0) < 2.06$ GeV/$c^2$ for all three signal channels.

① According to conservation of angular momentum laws, distribution of signal events in helicity angle is

Signal $\cos\theta_H$ distribution $\propto 1-\cos^2\theta_H$

②

- For $\rho^0$ & $\bar{K}^{*0}$ modes,

restrict $-0.8 < \cos\theta_H < 0.4$
to suppress backgrounds that peak at the edges of the distribution

- For $\phi$,

Background levels are lower overall
→entire range is used

③ $1.67 < M(D^0) < 2.06\ GeV/c^2$ for all three channels
$m(D^0) = 1.865\ GeV/c^2$ is the middle point

# Signal extraction and fit for $M(D^0)$

The invariant mass distribution of signal events is modeled with a Crystal-Ball probability density function [28] (PDF) for the $\rho^0$ and $\phi$ modes, and with the sum of a Crystal-Ball function and two Gaussians for the $K^{*0}$ mode. To take into account possible differences between MC calculations and data, a free offset and scale factor are implemented for the mean and width of the $\bar{K}^{*0}$ PDF, respectively. The obtained values are applied to the other two modes.

| $M(D^0)$ distribution | Model |
|---|---|
| $\rho^0$ mode | Crystal-Ball |
| $\phi$ mode | |
| $\overline{K}^{*0}$ mode | Sum of a Crystal-Ball, two Gaussians |

Crystal-ball function

$$f(x;\alpha,n,\bar{x},\sigma) = N \cdot \begin{cases} \exp(-\frac{(x-\bar{x})^2}{2\sigma^2}), & \text{for } \frac{x-\bar{x}}{\sigma} > -\alpha \\ A \cdot (B - \frac{x-\bar{x}}{\sigma})^{-n}, & \text{for } \frac{x-\bar{x}}{\sigma} \leqslant -\alpha \end{cases}$$

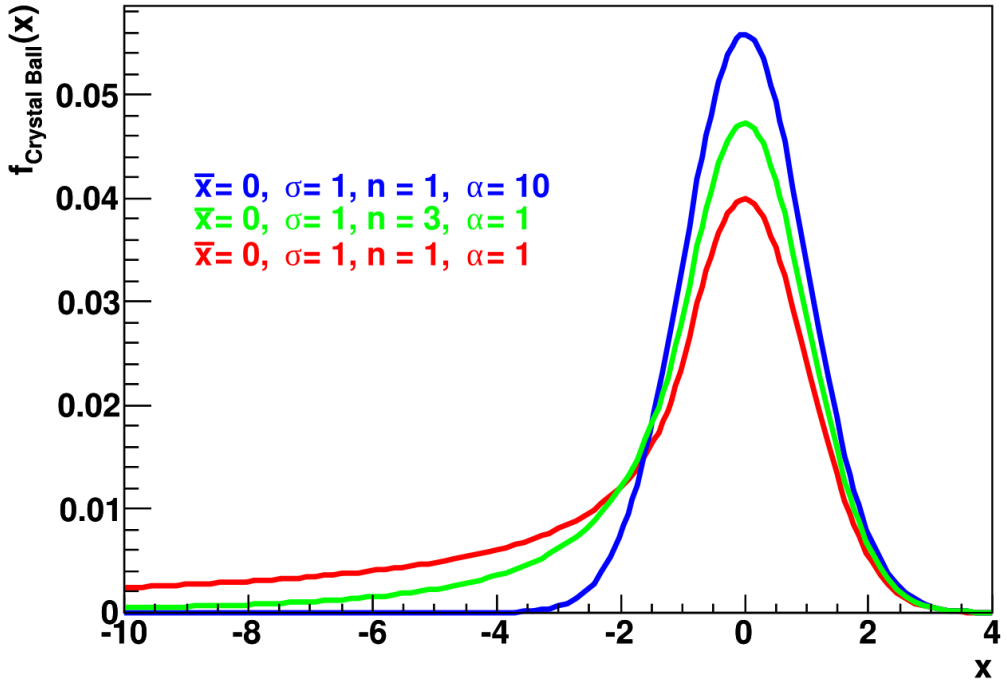

# Signal extraction and fit for $M(D^0)$

The invariant mass distribution of signal events is modeled with a Crystal-Ball probability density function [28] (PDF) for the $\rho^0$ and $\phi$ modes, and with the sum of a Crystal-Ball function and two Gaussians for the $\bar{K}^{*0}$ mode. To take into account possible differences between MC calculations and data, a free offset and scale factor are implemented for the mean and width of the $\bar{K}^{*0}$ PDF, respectively. The obtained values are applied to the other two modes.

To reduce difference between MC and data, use

- Free offset
- Scale factor

- Why applied to $\rho^0, \phi$ modes with obtained values from "$\bar{K}^{*0}$ mode"?

# Signal extraction and fit for $M(D^0)$

## $M(D^0)$ distribution of $\pi^0$ ($\eta$) background:

The $\pi^0$- and $\eta$-type background $M(D^0)$ distributions are described with a pure Crystal-Ball function or the sum of either a Crystal-Ball function or logarithmic Gaussian [29] and up to two additional Gaussians. For the $\rho^0$ mode, the $\pi^0$-type backgrounds are $\rho^0\pi^0$, $\rho^\pm\pi^\mp$, and $K^-\rho^+$ with the kaon being misidentified as a pion. For the $\phi$ mode, the only $\pi^0$-type background is the decay $D^0 \to \phi\pi^0$. For the $\bar{K}^{*0}$ mode, the $\pi^0$- and $\eta$-type backgrounds are the decays $D^0 \to \bar{K}^{*0}\pi^0$, $K^-\rho^+$, $K_0^*(1430)^-\pi^+$, $K^{*-}\pi^+$, nonresonant $K^-\pi^+\pi^0$, $\bar{K}^{*0}\eta$, and nonresonant $K^-\pi^+\eta$. In all

Logarithmic Gaussian function

$$f_X(x) = \frac{1}{x\sigma\sqrt{2\pi}} \exp\left(-\frac{(\ln x - \mu)^2}{2\sigma^2}\right).$$

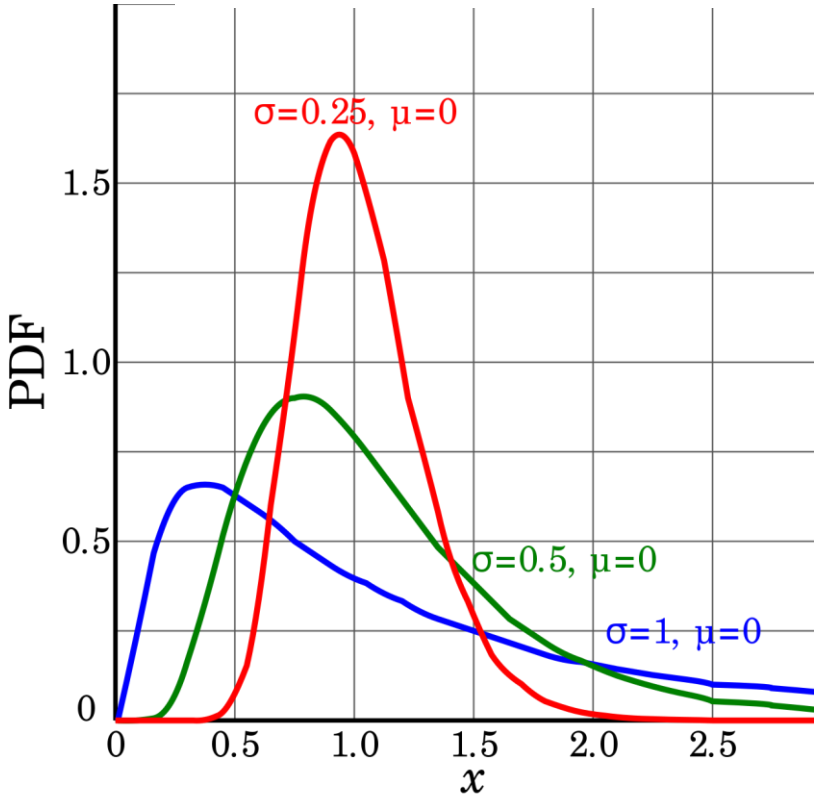

# Signal extraction and fit for $M(D^0)$

## $M(D^0)$ distribution of $\pi^0$ ($\eta$) background:

The $\pi^0$- and $\eta$-type background $M(D^0)$ distributions are described with a pure Crystal-Ball function or the sum of either a Crystal-Ball function or logarithmic Gaussian [29] and up to two additional Gaussians. For the $\rho^0$ mode, the $\pi^0$-type backgrounds are $\rho^0\pi^0$, $\rho^{\pm}\pi^{\mp}$, and $K^-\rho^+$ with the kaon being misidentified as a pion. For the $\phi$ mode, the only $\pi^0$-type background is the decay $D^0 \to \phi\pi^0$. For the $\bar{K}^{*0}$ mode, the $\pi^0$- and $\eta$-type backgrounds are the decays $D^0 \to \bar{K}^{*0}\pi^0$, $K^-\rho^+$, $K_0^*(1430)^-\pi^+$, $K^{*-}\pi^+$, nonresonant $K^-\pi^+\pi^0$, $\bar{K}^{*0}\eta$, and nonresonant $K^-\pi^+\eta$. In all

| Mode | $\pi^0$-type background | $\eta$-type background |
|---|---|---|
| $\rho^0$ | $\rho^0\pi^0, \rho^{\pm}\pi^{\mp}, K^-\rho^+$ | |
| $\phi$ | $\phi\pi^0$ | |
| $\bar{K}^{*0}$ | $\bar{K}^{*0}\pi^0, K^-\rho^+, \bar{K}^{*0}(1430)\pi^+$ $,\bar{K}^{*-}\pi^+$, nonresonant $K^-\pi^+\pi^0$ | $\bar{K}^{*0}\eta, K^-\pi^+\eta$ |

# Signal extraction and fit for $M(D^0)$

## Other-$D^0$ background:

In all three signal modes, the "other-$D^0$" background comprises all other decays wherein the $D^0$ is reconstructed from the majority of daughter particles. In the $\rho^0$ ($\bar{K}^{*0}$) mode, there are two additional small backgrounds: $\pi^+\pi^-(K^-\pi^+)$ with the photon being emitted as final state radiation (FSR), and $K^-\rho^+$ with the photon arising from the radiative decay of the charged $\rho$ meson. As there are no missing particles, these decays exhibit the same $M(D^0)$ distribution as the signal decays. We jointly denote them as irreducible background. Their yields are fixed to MC expectations and the known branching fractions [22]. The remaining combinatorial background is parametrized in $M(D^0)$ with an exponential function in the $\phi$ mode and a second-order Chebyshev polynomial in the $\rho^0$ and $\bar{K}^{*0}$ modes. All parameters describing the combinatorial background are allowed to vary in the fit. Possible correlations among the fit variables are negligible, except for the $\bar{K}^{*0}\pi^0$ and $K^-\rho^+$ backgrounds in the $\bar{K}^{*0}$ mode that are accommodated with an additional Gaussian in the mass PDF whose relative contribution is a function of $\cos\theta_H$.

## Irreducible background in $\rho^0(\bar{K}^{*0})$ mode

1. $\pi^+\pi^-(K^-\pi^+)$ with the photon being emitted as final state radiation(FSR)
2. $K^-\rho^+$ with the photon arising from radiative decay of charged $\rho$ meson ??

$B(\rho^\pm \to \pi^\pm\pi^0) \approx 100\%$

$B(\rho^\pm \to \pi^\pm\gamma) \approx (4.5 \pm 0.5) \times 10^{-4}$

# Signal extraction and fit for $M(D^0)$

## $M(D^0)$ distribution of $\pi^0$ ($\eta$) background:

The $M(D^0)$ PDF shape for the $\pi^0(\eta)$-type background, obtained from MC samples, is calibrated using the forbidden decay $D^0 \to K^0_S\gamma$, which yields mostly background from $D^0 \to K^0_S\pi^0$ and $D^0 \to K^0_S\eta$. The same PID criteria as for signal decays are applied, along with the $q$ and $p_{\rm CMS}(D^{*+})$ requirements as determined for the $\phi$ mode. The $K^0_S \to \pi^+\pi^-$ candidates in a $\pm 9$ MeV/$c^2$ window around the nominal mass are accepted. To calibrate the distribution, the simulated shape is smeared with a Gaussian function of width $7 \pm 1$ MeV/$c^2$ and an offset $(-1.33 \pm 0.25)$ MeV/$c^2$.

# $M(D^0)$ distribution

Figure 1 shows the signal-enhanced $M(D^0)$ projections of the combined sample in the region $-0.3 < \cos\theta_H < 0.3$ for all three signal modes, as well as the signal-enhanced $\cos\theta_H$ projection in the $1.85 < M(D^0) < 1.88$ GeV/$c^2$ region for the $\phi\gamma$ mode [30].

$D^0 \to \rho^0\gamma$

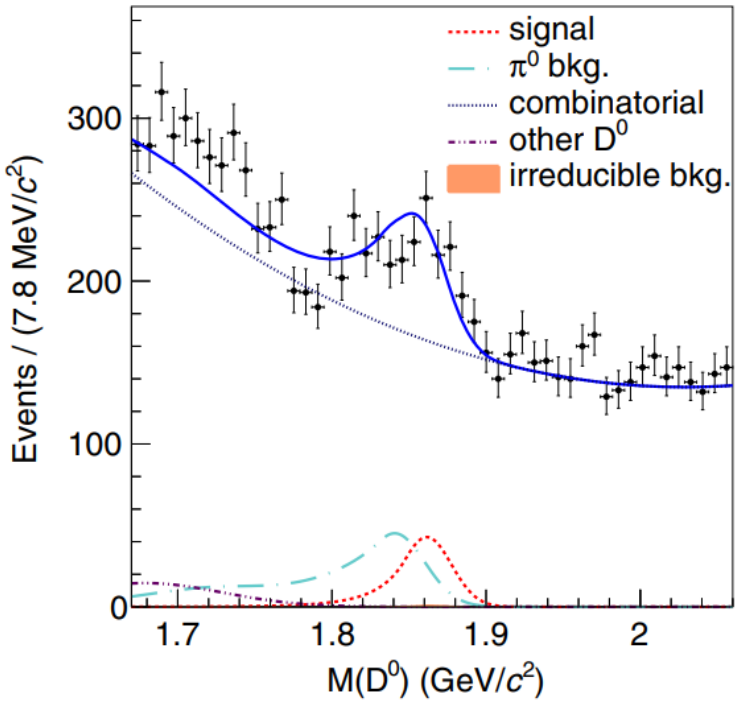


Shape of Signal: Crystal-Ball
Irreducible background were said before

$D^0 \to \bar{K}^{*0}\gamma$

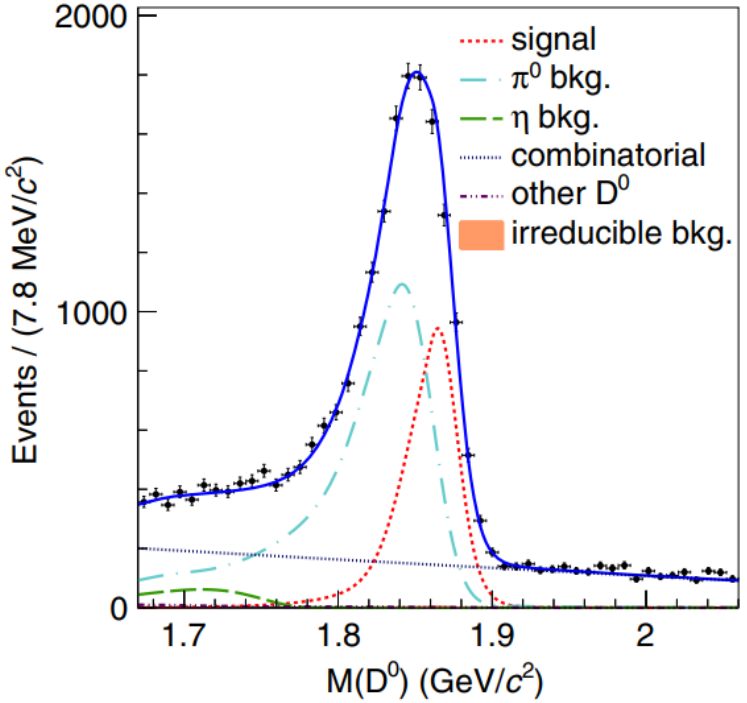


Crystal-Ball + 2 Gaussians

$D^0 \to \phi\gamma$

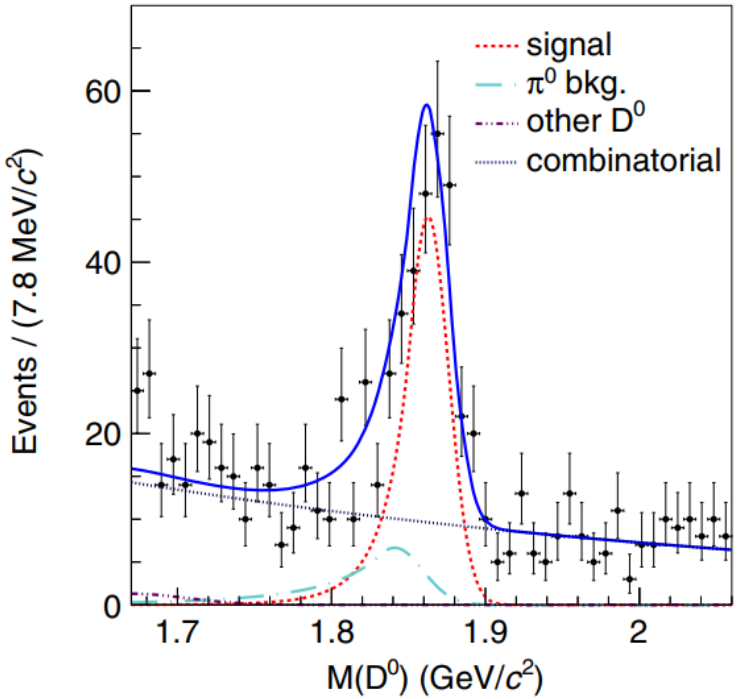


Crystal-Ball

# Fit for $\cos\theta_H$

## $\cos\theta_H$ distribution

The $\cos\theta_H$ signal distribution is parametrized as $1-\cos^2\theta_H$ for all three modes. For the $V\pi^0$ and $V\eta$ ($V=\rho^0,\phi,\bar{K}^{*0}$) categories, the shape is close to $\cos^2\theta_H$ and described with a second- ($\rho^0$ and $\phi$ mode) or third-order ($\bar{K}^{*0}$ mode) Chebyshev polynomial. In the $\phi$ mode, a linear term in $\cos\theta_H$ is added with a free coefficient to take into account possible interference between resonant and nonresonant amplitudes. For other background categories, the distributions are modeled using suitable PDFs based on MC predictions.

Figure 1 shows the signal-enhanced $M(D^0)$ projections of the combined sample in the region $-0.3 < \cos\theta_H < 0.3$ for all three signal modes, as well as the signal-enhanced $\cos\theta_H$ projection in the $1.85 < M(D^0) < 1.88$ GeV/$c^2$ region for the $\phi\gamma$ mode [30].

$D^0 \to \phi\gamma$

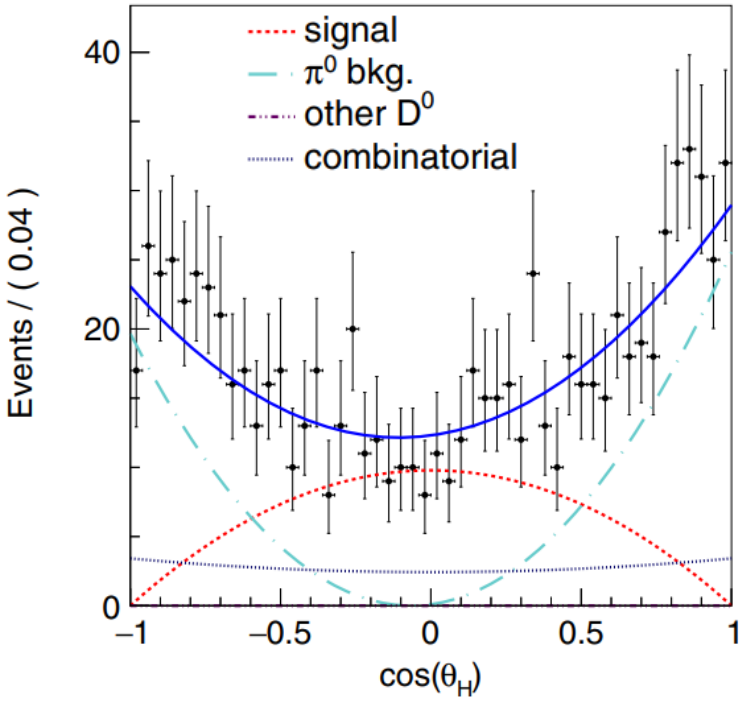


Signal $\propto 1-\cos^2\theta_H$

Background $\propto \cos^2\theta_H$

# Fit for $\cos\theta_H$

The $\cos\theta_H$ signal distribution is parametrized as $1-\cos^2\theta_H$ for all three modes. For the $V\pi^0$ and $V\eta$ ($V=\rho^0,\phi,\bar{K}^{*0}$) categories, the shape is close to $\cos^2\theta_H$ and described with a second- ($\rho^0$ and $\phi$ mode) or third-order ($\bar{K}^{*0}$ mode) Chebyshev polynomial. In the $\phi$ mode, a linear term in $\cos\theta_H$ is added with a free coefficient to take into account possible interference between resonant and nonresonant amplitudes. For other background categories, the distributions are modeled using suitable PDFs based on MC predictions.

Signal: parameterized as $1-\cos^2\theta_H$

Background for $V\pi^0, V\eta \propto \cos^2\theta_H$

| Mode | $\pi^0(\eta)$-type background | note |
|---|---|---|
| $\rho^0$ | $2^{nd}$-order Chebyshev poly | |
| $\phi$ | $2^{nd}$—order Chebyshev poly | Linear term added? |
| $\bar{K}^{*0}$ | $3^{rd}$-order Chebyshev poly | |

The **Chebyshev polynomials of the first kind** are obtained from the recurrence relation

$$T_0(x) = 1$$
$$T_1(x) = x$$
$$T_{n+1}(x) = 2x\,T_n(x) - T_{n-1}(x).$$

where $x = \cos\theta$

# Analysis of normalization modes

The analysis of the normalization modes relies on the previous analysis by Belle [31]. The same selection criteria as for signal modes for PID, vertex fit, $q$, and $p_{\mathrm{CMS}}(D^{*+})$ are applied. The signal yield is extracted by subtracting the background in a signal window of $M(D^0)$, where the background is estimated from a symmetrical upper and lower sideband. The signal window and sidebands for the $\pi^+\pi^-$ mode are $\pm 15$ and $\pm(20\text{–}35)$ MeV$/c^2$ around the nominal value [22], respectively. For the $K^+K^-$ mode, the signal window is $\pm 14$ MeV$/c^2$ and sidebands are $\pm(31\text{–}45)$ MeV$/c^2$, whereas for the $K^-\pi^+$ mode, the signal window is $\pm 16.2$ MeV$/c^2$ and sidebands are $\pm(28.8\text{–}45.0)$ MeV$/c^2$. The obtained signal yields and raw asymmetries are also listed in Table I.

# Systematic uncertainties

1. Since a relative calculation **using normalization channels**,
many systematic uncertainties **due to reconstruction efficiencies can cancel out**

2. Another systematic uncertainties arises from the specific analysis,
e.g. the method of **signal extraction**

3. Finally, a systematic uncertainty due to **nominal** $Br$ and $A_{\mathrm{CP}}$

- As resolution of fitted variables **for Belle and Belle 2**, performance of $\pi^0$ veto is **similar**

- As $A_{CP}$ measurements are relative to **normalization modes**,

**most systematic uncertainties should cancel**.
→ Thus overall systematic error for Belle 2 should be similar to Belle(ref: Belle 2 physics book)

- Details needs to be study and learn myself..

# Systematic uncertainties

TABLE II. Systematic uncertainties for all three signal modes.

| | $\sigma(\mathcal{B})/\mathcal{B}$ (%) | | | $A_{CP}$ ($\times 10^{-3}$) | | |
|---|---|---|---|---|---|---|
| | $\phi$ | $\bar{K}^{*0}$ | $\rho^0$ | $\phi$ | $\bar{K}^{*0}$ | $\rho^0$ |
| Efficiency | 2.8 | 3.3 | 2.8 | ... | ... | ... |
| Fit parametrization | 1.0 | 2.8 | 2.3 | 0.1 | 0.4 | 5.3 |
| Background normalization | ... | 0.3 | 0.6 | ... | 0.2 | 0.5 |
| Normalization mode | 0.0 | 0.0 | 0.1 | 0.5 | 0.0 | 0.3 |
| External $\mathcal{B}$ and $\mathcal{A}_{CP}$ | 2.0 | 1.0 | 1.8 | 1.2 | 0.0 | 1.5 |
| Total | 3.6 | 4.5 | 4.1 | 1.3 | 0.4 | 5.5 |

# Significance

We have conducted a measurement of the branching fraction and $\mathcal{A}_{CP}$ in three radiative charm decays $D^0 \to \rho^0\gamma$, $\phi\gamma$, and $\bar{K}^{*0}\gamma$ using the full data set recorded by the Belle experiment. We report the first observation of $D^0 \to \rho^0\gamma$ with a significance of $5.5\sigma$, including systematic uncertainties. The significance is calculated as $\sqrt{-2\ln(\mathcal{L}_0/\mathcal{L}_{\rm max})}$, where $\mathcal{L}_0$ is the likelihood value with the signal yield fixed to zero and $\mathcal{L}_{\rm max}$ is that of the nominal fit. The systematic uncertainties are included by convolving the statistical likelihood function with a Gaussian of width equal to the systematic uncertainty that affects the signal yield. The measured ratios of branching fractions to their normalization modes are $(1.25 \pm 0.21 \pm 0.05) \times 10^{-2}$, $(6.88 \pm 0.47 \pm 0.21) \times 10^{-3}$, and $(1.19 \pm 0.05 \pm 0.05) \times 10^{-2}$ for $D^0 \to \rho^0\gamma$, $\phi\gamma$, and $\bar{K}^{*0}\gamma$, respectively. The first uncertainty is statistical and the second is systematic. Using world-average values for the normalization modes [22], we obtain

# Results ($Br, A_{CP}$)

$$\mathcal{B}(D^0 \to \rho^0\gamma) = (1.77 \pm 0.30 \pm 0.07) \times 10^{-5},$$
$$\mathcal{B}(D^0 \to \phi\gamma) = (2.76 \pm 0.19 \pm 0.10) \times 10^{-5},$$
$$\mathcal{B}(D^0 \to \bar{K}^{*0}\gamma) = (4.66 \pm 0.21 \pm 0.21) \times 10^{-4}.$$

For the $\rho^0$ mode, the obtained value is considerably larger than theoretical expectations [34,35].

The result of the $\phi$ mode is improved compared to the previous determinations by Belle and *BABAR*, and is consistent with the world-average value [22].

Our branching fraction of the $\bar{K}^{*0}$ mode is $3.3\sigma$ above the *BABAR* measurement [12]. Both $\phi$ and $\bar{K}^{*0}$ results agree with the latest theoretical calculations [10].

$$\mathcal{A}_{CP}(D^0 \to \rho^0\gamma) = +0.056 \pm 0.152 \pm 0.006,$$
$$\mathcal{A}_{CP}(D^0 \to \phi\gamma) = -0.094 \pm 0.066 \pm 0.001,$$
$$\mathcal{A}_{CP}(D^0 \to \bar{K}^{*0}\gamma) = -0.003 \pm 0.020 \pm 0.000,$$

- They are consistent with no CP violation
- Uncertainty is statistically dominated,

→ the sensitivity can be greatly enhanced in Belle 2

# Results ($Br, A_{CP}$)

| | Int. luminosity | | | |
|---|---|---|---|---|
| | | $A_{CP}(D^0 \to \rho^0\gamma)$ | | |
| Belle result | $1\ ab^{-1}$ | $+0.056$ | $\pm0.152$ | $\pm0.006$ |
| | $5\ ab^{-1}$ | | $\pm0.07$ | |
| Belle II statistical error | $15\ ab^{-1}$ | | $\pm0.04$ | |
| | $50\ ab^{-1}$ | | $\pm0.02$ | |
| | | $A_{CP}(D^0 \to \phi\gamma)$ | | |
| Belle result | $1\ ab^{-1}$ | $-0.094$ | $\pm0.066$ | $\pm0.001$ |
| | $5\ ab^{-1}$ | | $\pm0.03$ | |
| Belle II statistical error | $15\ ab^{-1}$ | | $\pm0.02$ | |
| | $50\ ab^{-1}$ | | $\pm0.01$ | |
| | | $A_{CP}(D^0 \to \overline{K}^{*0}\gamma)$ | | |
| Belle result | $1\ ab^{-1}$ | $-0.003$ | $\pm0.020$ | $\pm0.000$ |
| | $5\ ab^{-1}$ | | $\pm0.01$ | |
| Belle II statistical error | $15\ ab^{-1}$ | | $\pm0.005$ | |
| | $50\ ab^{-1}$ | | $\pm0.003$ | |

Ref: belle 2 physics book

# Summary about the paper

- First observation of $D^0 \to \rho^0\gamma$

: $B(D^0 \to \rho^0\gamma) = (1.77 \pm 0.30 \pm 0.07) \times 10^{-5}$)

- First search for CP violation in decays $D^0 \to \rho^0\gamma, \phi\gamma, \overline{K}^{*0}(892)\gamma$ using $943fb^{-1}$ Belle data

: $A_{CP}(D^0 \to \rho^0\,\gamma) = +0.056 \pm 0.152 \pm 0.006$

,$A_{CP}(D^0 \to \phi\gamma) = -0.094 \pm 0.066 \pm 0.001$

,$A_{CP}(D^0 \to \overline{K}^{*0}\gamma) = -0.003 \pm 0.020 \pm 0.000$

- Dominant background from $\boldsymbol{\pi^0}$ ($\boldsymbol{\eta}$) veto

- Used normalization modes respectively which were well known from Belle paper(2008)

# Summary

- Systematic uncertainties:

I. using **normalization** channels
II. from the **specific analysis**(e.g method of signal extraction)
III. due to **nominal** $Br$ and $A_{\mathrm{CP}}$

- Results: First observation of $D^0 \to \rho^0\gamma$, First search for CP violation in decays $D^0 \to \rho^0\gamma, \phi\gamma, \overline{K}^{*0}(892)\gamma$

- My motivation for $D^0 \to \mathrm{V}\gamma$ analysis in future:

I. More statistics will **reduce statistical uncertainties** in Belle 2($A_{\mathrm{CP}}$)
II. Can **contribute to NP** in charm sector
III. I want to study why $\boldsymbol{D \to \omega\gamma}$ haven't been observed and make more precision in measurement (especially in $D \to \rho^0\gamma$)
IV. Tara Nanut(now in LHCb) tried to analyze the radiative charm decay in LHCb(2018). But it is not sure whether it is ongoing.

# Backup

Slides 7~13

Within the standard model (SM), charge-parity ($CP$) violation in weak decays of hadrons arises due to a single irreducible phase in the Cabibbo-Kobayashi-Maskawa matrix [1] and is expected to be very small for charmed hadrons: up to a few $10^{-3}$ [2–4]. Observation of $CP$ violation above the SM expectation would be an indication of new physics. This phenomenon in the charm sector has been extensively probed in the past decade in many different decays [5], reaching a sensitivity below 0.1% in some cases [6]. The search for $CP$ violation in radiative charm decays is complementary to the searches that have been exclusively performed in hadronic or leptonic decays. Theoretical calculations [7,8] show that, in SM extensions with chromomagnetic dipole operators, sizable $CP$ asymmetries can be expected in $D^0 \to \phi\gamma$ and $\rho^0\gamma$ decays. No experimental results exist to date regarding $CP$ violation in any of the radiative $D$ decays.

Radiative charm decays are dominated by long-range nonperturbative processes that can enhance the branching fractions up to $10^{-4}$, whereas short-range interactions are predicted to yield rates at the level of $10^{-8}$ [9,10]. Measurements of branching fractions of these decays can therefore be used to test the QCD-based calculations of long-distance dynamics. The radiative decay $D^0 \to \phi\gamma$ was first observed by Belle [11] and later measured with increased precision by *BABAR* [12]. In the same study, *BABAR* made the observation of $D^0 \to \bar{K}^{*0}(892)\gamma$. As for $D^0 \to \rho^0\gamma$, CLEO II has set an upper limit on its branching fraction at $2 \times 10^{-4}$ [13].

In this Letter, we present the first observation of $D^0 \to \rho^0\gamma$, improved branching fraction measurements of $D^0 \to \phi\gamma$ and $\bar{K}^{*0}\gamma$, as well as the first search for $CP$ violation in all three decays. Inclusion of charge-conjugate modes is implied unless noted otherwise. The measurements are based on 943 fb$^{-1}$ of data collected at or near the $\Upsilon(nS)$ resonances ($n = 2, 3, 4, 5$) with the Belle detector [14,15], operating at the KEKB asymmetric-energy $e^+e^-$ collider [16,17]. The detector components relevant for our study are a tracking system comprising a silicon vertex detector and a 50-layer central drift chamber, a particle identification (PID) system that consists of a barrel-like arrangement of time-of-flight scintillation counters and an array of aerogel threshold Cherenkov counters, and a CsI(Tl) crystal-based electromagnetic calorimeter (ECL). All are located inside a superconducting solenoid coil that provides a 1.5 T magnetic field.

We use Monte Carlo (MC) events, generated using EVTGEN [18], JETSET [19], and PHOTOS [20], followed with a GEANT3 [21] based detector simulation, representing 6 times the data luminosity, to devise selection criteria and investigate possible sources of background. The selection optimization is performed by maximizing $S/\sqrt{S+B}$, where $S$ ($B$) is the number of signal (background) events in a signal window of the reconstructed $D^0$ invariant mass $1.8 < M(D^0) < 1.9$ GeV/$c^2$. The branching fraction of $D^0 \to \rho^0\gamma$ is set to $3 \times 10^{-5}$ in simulations in accordance with Ref. [7], while the branching fractions of the other two decay modes are set to their world-average values [22].

We reconstruct $D^0$ mesons by combining a $\rho^0$, $\phi$, or $\bar{K}^{*0}$ with a photon. The vector resonances are formed from $\pi^+\pi^-$ ($\rho^0$), $K^+K^-$ ($\phi$), and $K^-\pi^+$ ($\bar{K}^{*0}$) combinations. Charged particles are reconstructed in the tracking system. A likelihood ratio for a given track to be a kaon or pion is obtained by utilizing specific ionization in the central drift chamber, light yield from the aerogel threshold Cherenkov counters, and information from the time-of-flight scintillation counters. Photons are detected with the ECL and required to have energies of at least 540 MeV. To suppress events with two daughter photons from a $\pi^0$ decay forming a merged cluster, we restrict the ratio of the energy deposited in a $3 \times 3$ array of ECL crystals ($E_9$) and that in the enclosing $5 \times 5$ array ($E_{25}$) to be above 0.94. About 63% of merged clusters are rejected by this requirement. We retain candidate $\rho^0$, $\phi$, or $\bar{K}^{*0}$ resonances if their invariant masses are within 150, 11, or 60 MeV/c$^2$ of their nominal masses [22], respectively. The $D^0$ mesons are required to originate from $D^{*+} \to D^0\pi^+$ in order to identify the $D^0$ flavor and to suppress the combinatorial background. The associated track must satisfy the aforementioned pion-hypothesis requirement. The $D^0$ daughters are refitted to a common vertex, and the resulting $D^0$ and the slow pion candidate from $D^{*+}$ decay are constrained to originate from a common point within the interaction point region. Confidence levels exceeding $10^{-3}$ are required for both fits. To suppress combinatorial background, we restrict the energy released in the decay, $q \equiv M(D^{*+}) - M(D^0) - m(\pi^+)$, where $m$ is the nominal mass, to lie in a $\pm 0.6$ MeV/$c^2$ window around the nominal value [22]. To further reduce the combinatorial background contribution, we require the momentum of the $D^{*+}$ in the center-of-mass

Slides 14~22

system $[p_{\rm CMS}(D^{*+})]$ to exceed 2.72, 2.42, and 2.17 GeV/$c$ in the $\rho^0\gamma$, $\phi\gamma$, and $\bar{K}^{*0}\gamma$ modes, respectively.

We measure the branching fractions and $CP$ asymmetries of the aforementioned radiative decays relative to well-measured hadronic $D^0$ decays to $\pi^+\pi^-$, $K^+K^-$, and $K^-\pi^+$ for the $\rho^0$, $\phi$, and $\bar{K}^{*0}$ mode, respectively. The signal branching fraction is

$$\mathcal{B}_{\rm sig} = \mathcal{B}_{\rm norm} \times \frac{N_{\rm sig}}{N_{\rm norm}} \times \frac{\varepsilon_{\rm norm}}{\varepsilon_{\rm sig}}, \quad (1)$$

where $N$ is the extracted yield, $\varepsilon$ is the reconstruction efficiency, and $\mathcal{B}$ is the branching fraction for the corresponding mode. The raw asymmetry in decays of $D^0$ mesons to a specific final state $f$,

$$A_{\rm raw} = \frac{N(D^0 \to f) - N(\bar{D}^0 \to \bar{f})}{N(D^0 \to f) + N(\bar{D}^0 \to \bar{f})}, \quad (2)$$

depends not only on the $CP$ asymmetry, $\mathcal{A}_{CP} = [\mathcal{B}(D^0 \to f) - \mathcal{B}(\bar{D}^0 \to \bar{f})]/[\mathcal{B}(D^0 \to f) + \mathcal{B}(\bar{D}^0 \to \bar{f})]$, but also on the contributions from the forward-backward production asymmetry ($A_{\rm FB}$) [23–25] and the asymmetry due to different reconstruction efficiencies for positively and negatively charged particles ($A_\varepsilon^\pm$): $A_{\rm raw} = \mathcal{A}_{CP} + A_{\rm FB} + A_\varepsilon^\pm$. Here, we have used a linear approximation assuming all terms to be small. The last two terms can be eliminated using the same normalization mode as used in the branching fraction measurements:

$$\mathcal{A}_{CP}^{\rm sig} = A_{\rm raw}^{\rm sig} - A_{\rm raw}^{\rm norm} + \mathcal{A}_{CP}^{\rm norm}, \quad (3)$$

where $\mathcal{A}_{CP}^{\rm norm}$ is the nominal value of $CP$ asymmetry of the normalization mode [5].

The dominant background arises from $D^0 \to f^+f^-\pi^0$ decays, with the $\pi^0$ subsequently decaying to a pair of photons, e.g., $D^0 \to \phi\pi^0(\to \gamma\gamma)$. If one of the daughter photons is missed in the reconstruction, the final state mimics the signal decay. Such events are suppressed with a dedicated $\pi^0$ veto in the form of a neural network [26] constructed from two mass-veto variables, described below. The signal photon is paired for the first (second) time with all other photons in the event having an energy greater than 30 (75) MeV. The pair in each set whose diphoton invariant mass lies closest to $m(\pi^0)$ is fed to the network. The final criterion on the veto variable rejects about 60% of background while retaining 85% of signal. With this method, we reject 13% more background at the same signal efficiency as compared to the veto used in previous Belle analyses [27]. A similar veto is considered for background from $\eta \to \gamma\gamma$, but is found to be ineffective due to the larger $\eta$ mass, which shifts the background further away from the signal peak.

We extract the signal yield and $CP$ asymmetry via a simultaneous unbinned extended maximum likelihood fit of $D^0$ and $\bar{D}^0$ samples to the invariant mass of the $D^0$ candidates and the cosine of the helicity angle $\theta_H$. The latter is the angle between the momenta of the $D^0$ and the $\pi^+$, $K^+$, or $K^-$ in the rest frame of the $\rho^0$, $\phi$, or $\bar{K}^{*0}$, respectively. By angular momentum conservation, the signal $\cos\theta_H$ distribution depicts a $1-\cos^2\theta_H$ dependence; no background contribution is expected to exhibit a similar shape. For the $\rho^0$ and $\bar{K}^{*0}$ modes, we restrict the helicity angle range to $-0.8 < \cos\theta_H < 0.4$ to suppress backgrounds that peak at the edges of the distribution. For the $\phi$ mode, where the background levels are lower overall, the entire $\cos\theta_H$ range is used. The $D^0$ candidate mass is restricted to $1.67 < M(D^0) < 2.06$ GeV/$c^2$ for all three signal channels.

The invariant mass distribution of signal events is modeled with a Crystal-Ball probability density function [28] (PDF) for the $\rho^0$ and $\phi$ modes, and with the sum of a Crystal-Ball function and two Gaussians for the $\bar{K}^{*0}$ mode. To take into account possible differences between MC calculations and data, a free offset and scale factor are implemented for the mean and width of the $\bar{K}^{*0}$ PDF, respectively. The obtained values are applied to the other two modes.

The $\pi^0$- and $\eta$-type background $M(D^0)$ distributions are described with a pure Crystal-Ball function or the sum of either a Crystal-Ball function or logarithmic Gaussian [29] and up to two additional Gaussians. For the $\rho^0$ mode, the $\pi^0$-type backgrounds are $\rho^0\pi^0$, $\rho^\pm\pi^\mp$, and $K^-\rho^+$ with the kaon being misidentified as a pion. For the $\phi$ mode, the only $\pi^0$-type background is the decay $D^0 \to \phi\pi^0$. For the $\bar{K}^{*0}$ mode, the $\pi^0$- and $\eta$-type backgrounds are the decays $D^0 \to \bar{K}^{*0}\pi^0$, $K^-\rho^+$, $K_0^*(1430)^-\pi^+$, $K^{*-}\pi^+$, nonresonant $K^-\pi^+\pi^0$, $\bar{K}^{*0}\eta$, and nonresonant $K^-\pi^+\eta$. In all three signal modes, the "other-$D^0$" background comprises all other decays wherein the $D^0$ is reconstructed from the majority of daughter particles. In the $\rho^0$ ($\bar{K}^{*0}$) mode, there are two additional small backgrounds: $\pi^+\pi^-(K^-\pi^+)$ with the photon being emitted as final state radiation (FSR), and $K^-\rho^+$ with the photon arising from the radiative decay of the charged $\rho$ meson. As there are no missing particles, these decays exhibit the same $M(D^0)$ distribution as the signal decays. We jointly denote them as irreducible background. Their yields are fixed to MC expectations and the known branching fractions [22]. The remaining combinatorial background is parametrized in $M(D^0)$ with an exponential function in the $\phi$ mode and a second-order Chebyshev polynomial in the $\rho^0$ and $\bar{K}^{*0}$ modes. All parameters describing the combinatorial background are allowed to vary in the fit. Possible correlations among the fit variables are negligible, except for the $\bar{K}^{*0}\pi^0$ and $K^-\rho^+$ backgrounds in the $\bar{K}^{*0}$ mode that are accommodated with an additional Gaussian in the mass PDF whose relative contribution is a function of $\cos\theta_H$.

Slides 22~

The $M(D^0)$ PDF shape for the $\pi^0(\eta)$-type background, obtained from MC samples, is calibrated using the forbidden decay $D^0 \to K^0_S\gamma$, which yields mostly background from $D^0 \to K^0_S\pi^0$ and $D^0 \to K^0_S\eta$. The same PID criteria as for signal decays are applied, along with the $q$ and $p_{\rm CMS}(D^{*+})$ requirements as determined for the $\phi$ mode. The $K^0_S \to \pi^+\pi^-$ candidates in a $\pm 9$ MeV/$c^2$ window around the nominal mass are accepted. To calibrate the distribution, the simulated shape is smeared with a Gaussian function of width $7 \pm 1$ MeV/$c^2$ and an offset $(-1.33 \pm 0.25)$ MeV/$c^2$.

The $\cos\theta_H$ signal distribution is parametrized as $1 - \cos^2\theta_H$ for all three modes. For the $V\pi^0$ and $V\eta$ ($V = \rho^0, \phi, \bar{K}^{*0}$) categories, the shape is close to $\cos^2\theta_H$ and described with a second- ($\rho^0$ and $\phi$ mode) or third-order ($\bar{K}^{*0}$ mode) Chebyshev polynomial. In the $\phi$ mode, a linear term in $\cos\theta_H$ is added with a free coefficient to take into account possible interference between resonant and nonresonant amplitudes. For other background categories, the distributions are modeled using suitable PDFs based on MC predictions.

Apart from normalizations, the asymmetries $A_{\rm raw}$ of signal and background modes are left free in the fit. All PDF shapes are fixed to MC values, unless previously stated otherwise.

In the $\bar{K}^{*0}$ mode, the yields (and $A_{\rm raw}$) of certain backgrounds that contain a small number of events (1 or 2 orders of magnitude less than signal) are fixed: $K^*_0(1430)^-\pi^+, K^{*-}\pi^+$, and the other-$D^0$ background. The same is done for backgrounds with a photon from FSR or radiative $\rho$ decay in the $\rho^0$ and $\bar{K}^{*0}$ modes. All fixed yields are scaled by the ratio between reconstructed signal events in data and simulation of the normalization modes. We impose an additional constraint in the $\bar{K}^{*0}$ mode by assigning two common $A_{\rm raw}$ variables to $\pi^0$- and $\eta$-type backgrounds, respectively. Since all are Cabibbo-favored decays, $\mathcal{A}_{CP}$ is expected to be zero, while other asymmetries contributing to $A_{\rm raw}$ are the same for decays with the same final-state particles.

Figure 1 shows the signal-enhanced $M(D^0)$ projections of the combined sample in the region $-0.3 < \cos\theta_H < 0.3$ for all three signal modes, as well as the signal-enhanced $\cos\theta_H$ projection in the $1.85 < M(D^0) < 1.88$ GeV/$c^2$ region for the $\phi\gamma$ mode [30]. The obtained signal yields and raw asymmetries are listed in Table I, along with reconstruction efficiencies. The background raw asymmetries are consistent with zero.

The analysis of the normalization modes relies on the previous analysis by Belle [31]. The same selection criteria as for signal modes for PID, vertex fit, $q$, and $p_{\rm CMS}(D^{*+})$ are applied. The signal yield is extracted by subtracting the background in a signal window of $M(D^0)$, where the background is estimated from a symmetrical upper and lower sideband. The signal window and sidebands for the

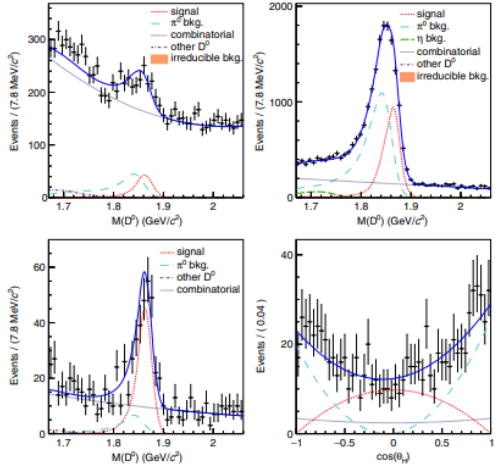


FIG. 1. The top two panels are signal-enhanced projections of the combined $M(D^0)$ distribution for $D^0 \to \rho^0\gamma$ (left) and $\bar{K}^{*0}\gamma$ (right). The bottom two panels are the signal-enhanced $M(D^0)$ (left) and $\cos\theta_H$ (right) distributions for $D^0 \to \phi\gamma$. Fit results are superimposed, with the fit components identified in the panel legend.

$\pi^+\pi^-$ mode are $\pm 15$ and $\pm(20$–$35)$ MeV/$c^2$ around the nominal value [22], respectively. For the $K^+K^-$ mode, the signal window is $\pm 14$ MeV/$c^2$ and sidebands are $\pm(31$–$45)$ MeV/$c^2$, whereas for the $K^-\pi^+$ mode, the signal window is $\pm 16.2$ MeV/$c^2$ and sidebands are $\pm(28.8$–$45.0)$ MeV/$c^2$. The obtained signal yields and raw asymmetries are also listed in Table I.

The systematic uncertainties are listed in Table II. All uncertainties are simultaneously estimated for $\mathcal{B}$ and $\mathcal{A}_{CP}$, unless stated otherwise. There are two main sources: those due to the selection criteria and those arising from the signal extraction method, both for signal and normalization modes. Some of the uncertainties from the first group cancel if they are common to the signal and respective normalization mode, such as those related to the PID, vertex fit, and requirement on $p_{\rm CMS}(D^{*+})$. A 2.2% uncertainty is ascribed to photon reconstruction efficiency [32].

TABLE I. Efficiencies, extracted yields, and $A_{\rm raw}$ values for all signal and normalization modes. The uncertainties are statistical.

| | Efficiency (%) | Yield | $A_{\rm raw}$ |
|---|---|---|---|
| $\rho^0\gamma$ | $6.77 \pm 0.09$ | $500 \pm 85$ | $+0.064 \pm 0.152$ |
| $\phi\gamma$ | $9.77 \pm 0.10$ | $524 \pm 35$ | $-0.091 \pm 0.066$ |
| $\bar{K}^{*0}\gamma$ | $7.81 \pm 0.03$ | $9104 \pm 396$ | $-0.002 \pm 0.020$ |
| $\pi^+\pi^-$ | $21.4 \pm 0.12$ | $(1.28 \pm 0.01) \times 10^5$ | $(8.1 \pm 3.0) \times 10^{-3}$ |
| $K^+K^-$ | $22.7 \pm 0.12$ | $(3.62 \pm 0.01) \times 10^5$ | $(2.2 \pm 1.7) \times 10^{-3}$ |
| $K^-\pi^+$ | $27.0 \pm 0.13$ | $(4.02 \pm 0.02) \times 10^5$ | $(1.3 \pm 0.5) \times 10^{-3}$ |

Slides 22~

TABLE II. Systematic uncertainties for all three signal modes.

| | $\sigma(\mathcal{B})/\mathcal{B}$ (%) | | | $A_{CP}$ ($\times 10^{-3}$) | | |
|---|---|---|---|---|---|---|
| | $\phi$ | $\bar{K}^{*0}$ | $\rho^0$ | $\phi$ | $\bar{K}^{*0}$ | $\rho^0$ |
| Efficiency | 2.8 | 3.3 | 2.8 | ... | ... | ... |
| Fit parametrization | 1.0 | 2.8 | 2.3 | 0.1 | 0.4 | 5.3 |
| Background normalization | ... | 0.3 | 0.6 | ... | 0.2 | 0.5 |
| Normalization mode | 0.0 | 0.0 | 0.1 | 0.5 | 0.0 | 0.3 |
| External $\mathcal{B}$ and $\mathcal{A}_{CP}$ | 2.0 | 1.0 | 1.8 | 1.2 | 0.0 | 1.5 |
| Total | 3.6 | 4.5 | 4.1 | 1.3 | 0.4 | 5.5 |

Because of the presence of the photon in the signal modes, the resolution of the $q$ distribution is worse than in the normalization modes. Thus, the related uncertainties cannot be assumed to cancel completely. We separately estimate the uncertainty due to the $q$ requirement using the control channel $D^0 \to \bar{K}^{*0}\pi^0$. For both MC calculations and data, the efficiency is estimated by calculating the ratio $R$ of the signal yield, extracted with and without the requirement on $q$. Then, the double ratio $R_{\rm MC}/R_{\rm data}$ is calculated to assess the possible difference between simulation and data. We obtain $R_{\rm MC}/R_{\rm data}(q) = 1.0100 \pm 0.0016$. We do not correct the efficiency by the central value; instead, we assign a systematic uncertainty of 1.16%.

The double-ratio method is also used to estimate the uncertainty due to the $\pi^0$-veto requirement on the control channel $D^0 \to K^0_S\pi^0$. The veto is calculated by pairing the first daughter photon (the more energetic one) of the $\pi^0$ with all others, but for the second daughter. The ratio $R$ of so-discarded events is calculated for MC calculations and data, with all other selection criteria applied. The obtained double ratio is $R_{\rm MC}/R_{\rm data}(\pi^0{\rm veto}) = 1.002 \pm 0.005$. The error directly translates to the systematic uncertainty of the efficiency.

The systematic uncertainties due to the $E_9/E_{25}$ and $E_\gamma$ requirements are estimated on the $\bar{K}^{*0}$ mode by repeating the fit without any constraint on the variable in question. The systematic error is the difference between the central value of the ratio $N_{\rm sig}/\varepsilon_{\rm sig}$ from this fit and that of the nominal fit. The obtained uncertainties are 0.23% for $E_9/E_{25}$ and 1.15% for $E_\gamma$.

The systematic uncertainties due to the requirement on the mass of the vector meson are estimated using the mass distribution, modeled with a relativistic Breit-Wigner function. In the signal window, we compare the integrals of the nominal function and the same modified by the uncertainties on the central value and width. The obtained uncertainties are 0.2% for the $\rho^0$ mode, 0.1% for the $\phi$ mode, and 1.7% for the $\bar{K}^{*0}$ mode. All uncertainties described above are summed in quadrature and the final value is listed as "Efficiency" in Table II. They affect only the branching fraction, as they cancel in Eq. (2).

For the fit procedure, a systematic uncertainty must be ascribed to every parameter that is determined and fixed to MC values but might differ in data. The fit procedure is repeated with each parameter varied by its uncertainty on the positive and negative sides. The larger deviation from the nominal branching fraction or $\mathcal{A}_{CP}$ value is taken as the double-sided systematic error and these are summed in quadrature for all parameters. An uncertainty is assigned to the calibration offset and width of the $\pi^0$-type backgrounds. For the $\phi$ and $\rho^0$ modes, the uncertainty is calculated for the width scale factor (and offset) of the signal $M(D^0)$ PDF and $\pi^0$-type background varied simultaneously. All these quadratically summed uncertainties are listed as "Fit parametrization" in Table II.

The values of the fixed yields of some backgrounds in the $\rho^0$ and $\bar{K}^{*0}$ mode are varied according to the uncertainties of the respective branching fractions [22]. For the category with the FSR photon, a 20% variation is used [33]. As the branching fractions contributing to the other-$D^0$ background in the $\bar{K}^{*0}$ mode are unknown, we apply the largest variation from among other categories. The quadratically summed uncertainty is listed as "Background normalization" in Table II.

For the normalization modes, the procedure is repeated with shifted sidebands, starting from $\pm 25$ MeV/$c^2$ from the nominal $m(D^0)$ value. The statistical error from sideband subtraction is taken into account. Since possible differences in the signal shape between simulation and data could also affect the signal yield, a similar procedure as for the calibration of the $\pi^0$ background is performed. A systematic uncertainty is assigned for the case when the MC shape is smeared by a Gaussian of width 1.6 MeV/$c^2$. All uncertainties arising from normalization modes are summed in quadrature and listed as "Normalization mode" in Table II.

Finally, an uncertainty is assigned by varying the nominal values of the branching fractions and $\mathcal{A}_{CP}$ of the normalization modes and vector meson subdecay modes by their respective uncertainties.

We have conducted a measurement of the branching fraction and $\mathcal{A}_{CP}$ in three radiative charm decays $D^0 \to \rho^0\gamma$, $\phi\gamma$, and $\bar{K}^{*0}\gamma$ using the full data set recorded by the Belle experiment. We report the first observation of $D^0 \to \rho^0\gamma$ with a significance of $5.5\sigma$, including systematic uncertainties. The significance is calculated as $\sqrt{-2\ln(\mathcal{L}_0/\mathcal{L}_{\rm max})}$, where $\mathcal{L}_0$ is the likelihood value with the signal yield fixed to zero and $\mathcal{L}_{\rm max}$ is that of the nominal fit. The systematic uncertainties are included by convolving the statistical likelihood function with a Gaussian of width equal to the systematic uncertainty that affects the signal yield. The measured ratios of branching fractions to their normalization modes are $(1.25 \pm 0.21 \pm 0.05) \times 10^{-2}$, $(6.88 \pm 0.47 \pm 0.21) \times 10^{-3}$, and $(1.19 \pm 0.05 \pm 0.05) \times 10^{-2}$ for $D^0 \to \rho^0\gamma$, $\phi\gamma$, and $\bar{K}^{*0}\gamma$, respectively. The first uncertainty is statistical and the second is systematic. Using world-average values for the normalization modes [22], we obtain

Slides 22~

$$\mathcal{B}(D^0 \to \rho^0\gamma) = (1.77 \pm 0.30 \pm 0.07) \times 10^{-5},$$
$$\mathcal{B}(D^0 \to \phi\gamma) = (2.76 \pm 0.19 \pm 0.10) \times 10^{-5},$$
$$\mathcal{B}(D^0 \to \bar{K}^{*0}\gamma) = (4.66 \pm 0.21 \pm 0.21) \times 10^{-4}.$$

For the $\rho^0$ mode, the obtained value is considerably larger than theoretical expectations [34,35]. The result of the $\phi$ mode is improved compared to the previous determinations by Belle and *BABAR*, and is consistent with the world-average value [22]. Our branching fraction of the $\bar{K}^{*0}$ mode is $3.3\sigma$ above the *BABAR* measurement [12]. Both $\phi$ and $\bar{K}^{*0}$ results agree with the latest theoretical calculations [10].

We also report the first measurement of $\mathcal{A}_{CP}$ in these decays. The values, obtained from Eq. (3),

$$\mathcal{A}_{CP}(D^0 \to \rho^0\gamma) = +0.056 \pm 0.152 \pm 0.006,$$
$$\mathcal{A}_{CP}(D^0 \to \phi\gamma) = -0.094 \pm 0.066 \pm 0.001,$$
$$\mathcal{A}_{CP}(D^0 \to \bar{K}^{*0}\gamma) = -0.003 \pm 0.020 \pm 0.000,$$

are consistent with no *CP* violation. Since the uncertainty is statistically dominated, the sensitivity can be greatly enhanced at the upcoming Belle II experiment [36].